

Observation of layer-dependent uniaxial charge density wave in a noble metal alloy superconductor β-$IrSn_4$

Xiao Liu(刘潇), Geng Li(李更), Shiwei Diao(刁世伟), Haisen Liu(刘海森), Zhen Zhao (赵振), Haitao Yang(杨海涛), Lizhi Zhang(张礼智), Xiao Lin(林晓), and Hong-Jun Gao(高鸿钧)

Citation: Chin. Phys. B, 2026, 35 (**8**): 087102. DOI: 10.1088/1674-1056/ae69c6
http://cpb.iphy.ac.cn; http://iopscience.iop.org/cpb

What follows is a list of articles you may be interested in

Fine electronic structure and 5f-electron localized-itinerant transition in uranium films

Yun Zhang(张云), Jian Wu(吴健), Ying Jiang(蒋颖), Qiuyun Chen(陈秋云), Wei Feng(冯卫), Xiangfei Yang(杨向飞), Qin Liu(刘琴), Xiegang Zhu(朱燮刚), Dengpeng Yuan(袁登鹏), Qiang Zhang(张强), Xinchun Lai(赖新春), Qunqing Hao(郝群庆), and Shiyong Tan(谭世勇)

Chin. Phys. B, 2026, 35 (**4**): 047102. DOI: 10.1088/1674-1056/ae101a

Strain tuning of charge density wave and Mott-insulating states in monolayer VTe_2

Wenqian Tu(涂文倩), Run Lv(吕润), Dingfu Shao(邵定夫), Yuping Sun(孙玉平), and Wenjian Lu(鲁文建)

Chin. Phys. B, 2025, 34 (**9**): 097103. DOI: 10.1088/1674-1056/ade8e0

Momentum-dependent anisotropy of the charge density wave gap in quasi-1D $ZrTe_{3-x}Se_x$ (x = 0.015)

Renjie Zhang(张任杰), Yudong Hu(胡裕栋), Yiwei Cheng(程以伟), Yigui Zhong(钟益桂), Xuezhi Chen(陈学智), Junqin Li(李俊琴), Kozo Okazaki, Yaobo Huang(黄耀波), Tian Shang(商恬), Shifeng Jin(金士锋), Baiqing Lv(吕佰晴), and Hong Ding(丁洪)

Chin. Phys. B, 2025, 34 (**7**): 077106. DOI: 10.1088/1674-1056/addcc5

Competing phases and suppression of superconductivity in hole-doped Hubbard model on honeycomb lattice

Hao Zhang(张浩), Shaojun Dong(董少钧), and Lixin He(何力新)

Chin. Phys. B, 2025, 34 (**7**): 077102. DOI: 10.1088/1674-1056/adcb20

Observation of a long-range unidirectional charge density wave in kagome superconductor KV_3Sb_5

Xingwei Shi(石兴伟), Xiao Liu(刘潇), Geng Li(李更), Zhen Zhao(赵振), Haitao Yang(杨海涛), Xiao Lin(林晓), and Hong-Jun Gao(高鸿钧)

Chin. Phys. B, 2025, 34 (**7**): 077101. DOI: 10.1088/1674-1056/add7ad

---

RAPID COMMUNICATION

Observation of layer-dependent uniaxial charge density wave in a noble metal alloy superconductor β-$IrSn_4$

Xiao Liu(刘潇)[1,2,†], Geng Li(李更)[1,2,3,†,‡] Shiwei Diao(刁世伟)[4,†], Haisen Liu(刘海森)[1,2], Zhen Zhao (赵振)[1,2], Haitao Yang(杨海涛)[1,2,3], Lizhi Zhang(张礼智)[4,§], Xiao Lin(林晓)[1,¶], and Hong-Jun Gao(高鸿钧)[1,2,3]

[1] *School of Physical Sciences, University of Chinese Academy of Sciences, Beijing* 100190, *China*

[2] *Beijing National Center for Condensed Matter Physics and Institute of Physics, Chinese Academy of Sciences, Beijing* 100190, *China*

[3] *Hefei National Laboratory, Hefei* 230088, *China*

[4] *Laboratory of Theoretical and Computational Nanoscience, National Center for Nanoscience and Technology, Beijing* 100190, *China*

(Received 8 April 2026; revised manuscript received 26 April 2026; accepted manuscript online 7 May 2026)

The AB_4-type intermetallic compounds host a wide range of emergent quantum phenomena, providing a fertile platform for exploring the interplay between crystal structure and electronic orders. Among them, β-$IrSn_4$ has recently attracted attention as a noble-metal-based layered superconductor with weak interlayer coupling and type-I superconductivity. However, its electronic states and possible symmetry-breaking orders remain largely unexplored on the atomic scale. Here, we report the observation of a layer-dependent uniaxial charge density wave (CDW) in β-$IrSn_4$ using ultra-low-temperature scanning tunneling microscopy. The charge order appears as stripe-like modulations that break the in-plane C_4 symmetry, and its orientation rotates by 90° between adjacent layers. Spectroscopy measurements reveal a homogeneous superconducting gap coexisting with the layer-dependent CDW, with no detectable modulation from the charge order. First-principles calculations suggest that interlayer coupling induces the observed anisotropic electronic structure. These results reveal a layer-dependent symmetry-breaking electronic state in β-$IrSn_4$ and highlight the role of interlayer interactions in shaping its electronic properties.

Keywords: charge density wave, layer-dependent, superconductivity, interlayer coupling

PACS: 71.45.Lr, 74.55.+v, 74.70.–b, 63.22.Np

DOI: 10.1088/1674-1056/ae69c6 **CSTR:** 32038.14.CPB.ae69c6

Intermetallic compounds with the AB_4 stoichiometry constitute an important class of quantum materials, exhibiting diverse phenomena such as superconductivity[1–8] and nontrivial electronic topology.[1–4,7–15] Their rich structural motifs, often featuring complex coordination environments and layered stacking sequences, provide a natural platform for studying how lattice symmetry, dimensionality, and electronic interactions intertwine. In particular, the sensitivity of these systems to subtle structural variations makes them ideal candidates for uncovering emergent symmetry-breaking states and their coupling to collective electronic phases.

Among these materials, β-$IrSn_4$ stands out as a recently revisited system with intriguing physical properties.[6–8,10,16] It crystallizes in a layered structure composed of $IrSn_8$ square antiprisms, giving rise to quasi-two-dimensional electronic characteristics with finite interlayer coupling. Transport and thermodynamic measurements have identified β-$IrSn_4$ as a type-I superconductor with an exceptionally low critical field,[6–8] suggesting a conventional BCS pairing mechanism. Meanwhile, its noble-metal-based composition and relatively weak electronic correlations distinguish it from many strongly correlated charge density wave (CDW) systems,[17–25] raising the fundamental question of whether and how symmetry-breaking electronic orders can emerge in such a setting. Despite these intriguing properties, direct experimental access to its atomic-scale electronic structure has remained scarce.

Here, we report an atomic-scale investigation of β-$IrSn_4$ using scanning tunneling microscopy and spectroscopy at dilution refrigerator temperatures. We uncover a uniaxial charge density wave that spontaneously breaks the in-plane C_4 symmetry into C_2, forming stripe-like electronic modulations along one crystallographic axis. More strikingly, by systematically probing multiple terraces corresponding to different layers in the stacking sequence, we reveal that the CDW orientation alternates by 90° between adjacent layers, giving rise to a layer-dependent uniaxial CDW. This behavior is strictly locked to the crystallographic stacking and cannot be attributed to surface effects, indicating an intrinsic bulk electronic order governed by interlayer interactions. Concurrent spectroscopic measurements demonstrate a homogeneous

[†]These authors contributed equally to this work.

[‡]Corresponding author. E-mail: gengli.iop@iphy.ac.cn

[§]Corresponding author. E-mail: zhanglz@nanoctr.cn

[¶]Corresponding author. E-mail: xlin@ucas.ac.cn

© 2026 Chinese Physical Society and IOP Publishing Ltd. All rights, including for text and data mining, AI training, and similar technologies, are reserved.

superconducting gap that is insensitive to the CDW, defects, and step edges, suggesting weak or negligible coupling between superconductivity and charge order. Supported by first-principles calculations, our results establish a direct link between interlayer coupling and anisotropic electronic structure, providing new insight into how three-dimensional stacking can stabilize unconventional symmetry-breaking states even in weakly correlated intermetallic systems.

High-quality β-$IrSn_4$ single crystals were synthesized via a self-flux growth method. Energy dispersive x-ray spectroscopy and single crystal x-ray diffraction (Fig. S1) were done to confirm that the sample was in the correct element ratio and in the β phase. β-$IrSn_4$ crystallizes in the space group $I4_1/acd$ (#142), featuring a layered structure (Fig. 1(a)). Each Ir atom is coordinated by eight Sn atoms forming an $IrSn_8$ square antiprism. These edge-sharing antiprisms stack in an A–B–C–D sequence along the c-axis to form the bulk crystal.

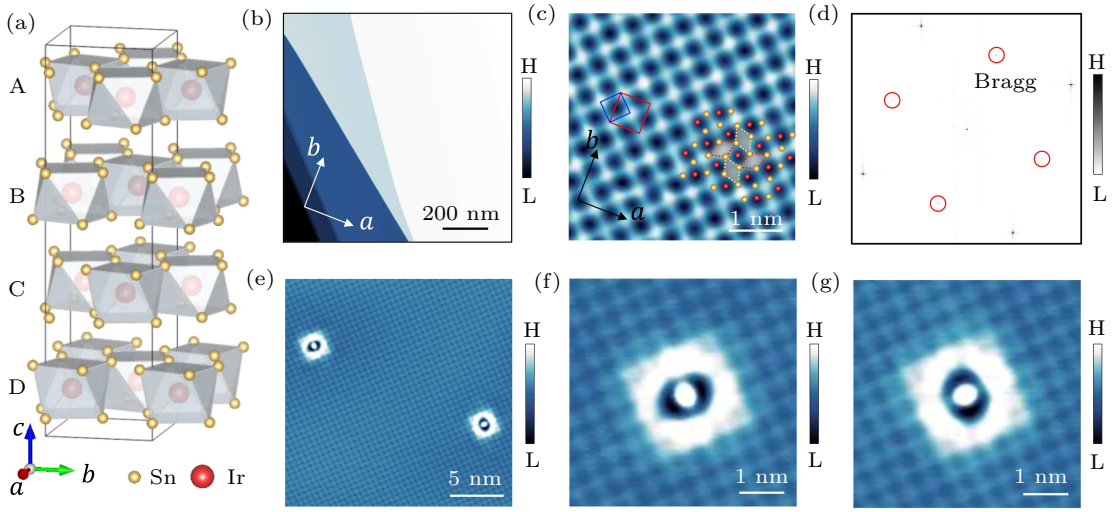


Fig. 1. Atomic model, surface topography and determination of as-cleaved Sn termination of β-$IrSn_4$. (a) Schematic illustration of the atomic structure of β-$IrSn_4$ with Ir and Sn atoms respectively denoted by red and yellow spheres. Each Ir atom is coordinated by a square antiprism (grey) formed by eight Sn atoms, with all $IrSn_8$ antiprisms interconnected through edge-sharing. The crystal structure shows an A–B–C–D stacking sequence along the c-axis. (b) STM topography of micron-scale atomically flat cleaved surface ($V_s = -90$ mV, $I_t = 50$ pA). (c) Atomically resolved STM images ($V_s = -600$ mV, $I_t = 1$ nA) showing a square lattice, with the schematic of an Ir atom layer and the subsequent Sn atom layer overlaid above. (d) FT of STM image of a typical area. Peaks corresponding to Bragg points (red circles) and Ir lattice (blue circles) are clearly visible, whose corresponding periodic units are represented by red and blue squares in panel (c). (e) STM image of two adatoms and their surrounding electronic states exhibiting perpendicular orientation ($V_s = 1$ V, $I_t = 1$ nA), whose equivalent positions are denoted by grey rhombi respectively bordered by red and yellow dashed lines in panel (c), which clarify two types of mutually perpendicular surface electronic environments. (f), (g) The zoom-in view of the two adatoms and their surrounding electronic states in panel (e).

Scanning tunneling microscopy/spectroscopy (STM/S) measurements were carried out in a customized STM system under an ultrahigh vacuum of 1×10^{-10} mbar. The temperature of the STM sample holder was lowered to 31 mK through ^{3}He–^{4}He dilution refrigeration. Tungsten tips, prepared by chemical etching, were annealed in ultrahigh vacuum to remove surface oxides and adsorbed contaminants, and subsequently calibrated on a clean Au(111) surface prior to use. The sample was mechanically cleaved at liquid nitrogen temperature in an ultrahigh vacuum environment and immediately transferred to the STM sample holder. Differential conductance was acquired using a standard lock-in technique at a frequency of 932 Hz with an excitation voltage of one percent of the sample bias for stabilizing the tunneling junction.

We begin by characterizing the surface atomic structure and termination of cleaved β-$IrSn_4$. Large-scale STM topography reveals micron-scale atomically flat terraces on the cleaved surface (Fig. 1(b)). Atomic-resolution STM imaging (Fig. 1(c)) and its Fourier transform (FT) (Fig. 1(d)) confirm a square surface lattice. The most prominent periodicity observed in the real-space image and the most pronounced peaks in the FT correspond to a lattice with a period of ~ 0.45 nm, consistent with the known periodicity of the Ir atomic layer according to previous studies.[6,7,16] However, cleavage is expected to occur between the Sn layers of adjacent sandwich layers due to their larger interlayer spacing and weaker bonding. The atomic-resolution STM patterns observed across all terraces show the same feature, and the step heights between terraces are integer multiples of $c/4$, indicating that the termination of cleavage is the Sn layer.

To further confirm the Sn-terminated surface, we found a type of adatom with surrounding C_2-symmetric electronic environments, which might be Sn or Ir atoms induced by the cleavage process. We also noticed that there is a sort of sites marked by the centers of the grey rhombi formed by four Sn atoms in Fig. 1(c) lying on two-fold rotation symmetry axes. Adjacent rhombi exhibit mutually perpendicular orientations, resulting in 90°-rotated electronic environments between neighboring rhombic centers, leading to a rule: traversing an *even* number of steps along adjacent rhombic

centers leads to identical electronic environments; traversing an *odd* number of steps yields perpendicular electronic environments. Intriguingly, two adatoms separated by 47 rhombic steps (Fig. 1(e)) display mutually perpendicular electronic states, while those separated by 8 steps (Fig. S2(a)) show parallel orientations. The consistent observation of the orientations of these adatoms at their expected positions unequivocally confirms that the cleaved surface is Sn-terminated, and the atomic correspondence between the STM topography and the surface atomic structure is thus established, as depicted in Fig. 1(c). Furthermore, defects with C_4 symmetry are found at the dark points of the STM topography (Fig. S2(b)), which cannot be pushed away by the tip like the adatoms in Fig. 1. We attribute these defects to single Ir atom vacancies in subsurface layers because Ir atomic sites uniquely exhibit local C_4 symmetry; the spatial coincidence of the black points in STM topography with Ir lattice sites gives further evidence of the aforementioned atomic correspondence. Unambiguously establishing this atomic registry through defect analysis is a crucial prerequisite, as it provides the exact structural input required for the subsequent theoretical modelling of the symmetry-breaking CDW state, which will be discussed later.

Further STM studies on the as-cleaved Sn-terminated surface of β-$IrSn_4$ reveal a striking symmetry-broken electronic state. Atomically resolved topography, acquired under smaller tip-sample distance ($\sim$ 200 mV), exhibits pronounced commensurate $1a_0$ uniaxial CDWs manifesting as stripe-like patterns (Fig. 2(a)). These stripes, consistently aligning along one of the two equivalent directions, the crystallographic a or b axis, selectively enhance or suppress the electronic states along specific Sn atom chains, which reduces the C_4 rotational symmetry to C_2 and breaks the mirror symmetry within the single sandwich layer. The anisotropic nature of this charge order is demonstrated by the FT of the STM image as well (Fig. 2(b)). The FT spectrum exhibits strongly anisotropic Bragg peaks, with significantly higher intensity along the direction parallel to the observed stripes compared to the orthogonal direction.

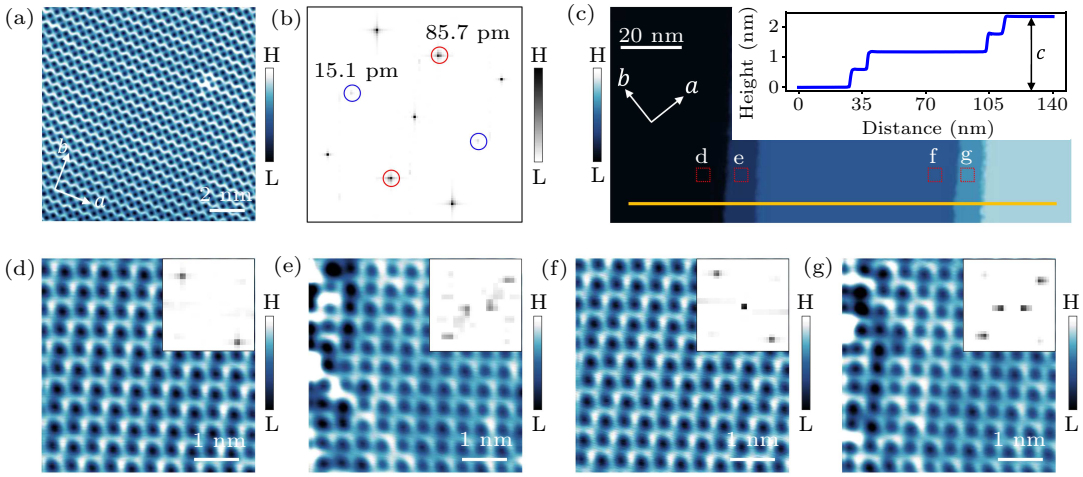


Fig. 2. Layer-dependent uniaxial charge density waves with perpendicular orientation. (a) Atomically resolved STM image showing uniaxial CDW stripes ($V_s = 200$ mV, $I_t = 1$ nA). (b) FT of the STM image in (a), exhibiting strongly anisotropic Bragg peaks with pronounced intensity contrast between orthogonal directions. (c) STM topography showing five consequent sandwich-layer terraces ($V_s = 1$ V, $I_t = 50$ pA). Inset: Height line profile at the yellow line, clarifying that the five terraces have height difference of a quarter of a unit cell consequently. (d)–(g) Zoom-in STM images at the corresponding red dashed square in panel (c) ($V_s = 200$ mV, $I_t = 7$ nA), showing alternating uniaxial CDW stripes with perpendicular orientation. Inset: FT image of each STM topography.

To investigate the evolution of this CDW state across different layers, we systematically probed a region containing five consecutive atomic terraces separated by steps (Fig. 2(c)). STM topographic imaging at each terrace level confirmed the atomically flat nature of each layer. The height line profile across these terraces (inset, Fig. 2(c)) revealed that the step height between consecutive terraces is consistently equal to a quarter of the unit cell parameter of c-axis ($c/4 \sim 0.3$ nm), corresponding to the separation between Sn-terminated layers within the A–B–C–D stacking sequence. High-resolution STM imaging performed under identical tunneling conditions on each individual terrace (Figs. 2(d)–2(g)) yielded a remarkable observation that the orientation of the uniaxial CDW stripes alternates between consecutive layers. Stripes on terraces separated by an odd multiple of the $c/4$ step height (e.g., between layers A and B, or B and C, etc.) exhibit perpendicular orientations. In contrast, stripes on terraces separated by an even multiple of the $c/4$ step height (e.g., between layers A and C, or B and D) share the same orientation. The FT of each individual terrace image (insets, Figs. 2(d)–2(g)) consistently reflects this layer-dependent anisotropy, confirming the CDW direction for each layer.

This observation of layer-dependent uniaxial CDW with perpendicular alignment between adjacent Sn-terminated layers is highly reproducible across different sample regions and step configurations (Fig. S3). The strict dependence of the CDW orientation alternation on the $c/4$ step height rule robustly excludes the possibility of this phenomenon arising

from artifacts related to the STM tip or from surface reconstructions confined to the topmost layer. Instead, it provides compelling evidence for an intrinsic, layer-dependent electronic ordering that breaks symmetry differently in consecutive layers of the β-$IrSn_4$ crystal.

The electronic properties of β-$IrSn_4$ at low temperatures were probed using scanning tunneling spectroscopy (STS) at dilution refrigerator temperature ($\sim$ 31 mK). Spectroscopy measurements (Fig. 3(b)) reveal a clear superconducting (SC) gap signature in the differential conductance ($\mathrm{d}I/\mathrm{d}V$) spectrum. The spectrum exhibits a V-shaped gap structure centered at the Fermi level, with coherence peaks located at approximately $\pm$0.5 mV. A numerical fit based on the Dynes model[26] (solid line in Fig. 3(b)) shows consistency with the experimental data. The yielded gap value Δ is 0.158 meV, resulting in a $2\Delta/k_{\mathrm{B}}T_{\mathrm{c}}$ ratio of 3.49 with the T_{c} assumed as 1.05 K reported by an earlier study.[7] This ratio closely matches the isotropic BCS weak-coupling limit where it is 3.53. This gap structure is consistently observed across the sample surface, existing simultaneously with the layer-dependent uniaxial CDW. A $\mathrm{d}I/\mathrm{d}V$ linecut across the CDW stripe is performed (Figs. 3(c) and 3(d)). To quantitatively evaluate the spatial uniformity of the superconductivity, we performed Dynes model fitting on each individual spectrum along the linecut to extract the local gap size Δ, which is overlaid in Figs. 3(c) and 3(d). The extracted Δ exhibits an extremely small standard deviation of 0.001 mV, representing an upper bound of spatial modulation of merely $\sim$ 0.63% relative to the average gap size. Such extraordinary spatial homogeneity establishes the weak or negligible coupling nature between the layer-dependent uniaxial CDW and the superconductivity.

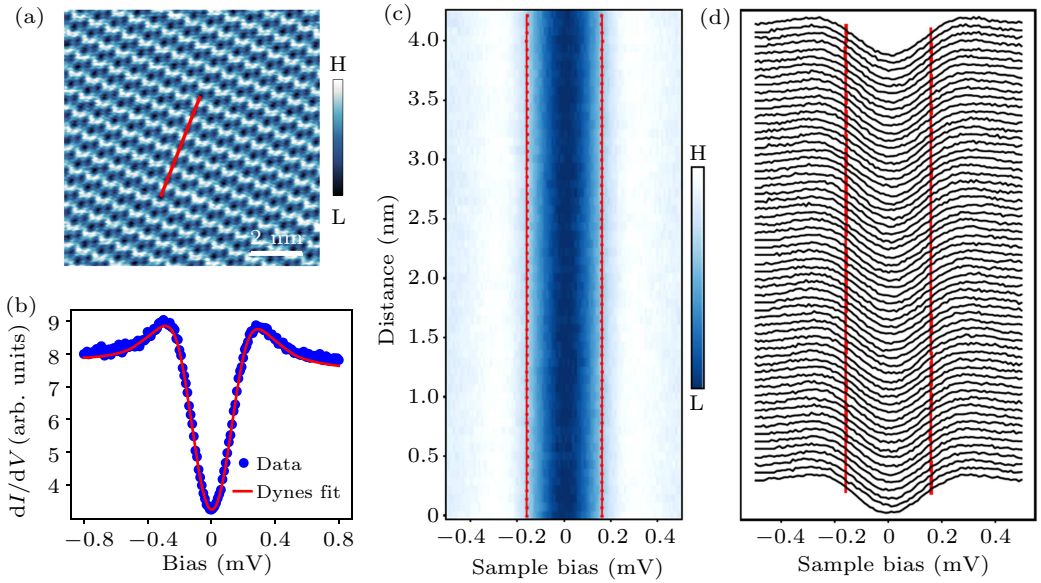


Fig. 3. Homogeneous superconductivity coexisting with uniaxial CDW stripes. (a) Atomically resolved STM image of a region with uniaxial CDW stripes ($V_{\mathrm{s}} = 200$ mV, $I_{\mathrm{t}} = 5$ nA). (b) Spatial average of 1024 $\mathrm{d}I/\mathrm{d}V$ spectra and Dynes fit of the data, showing good consistency. (c), (d) Pseudo color map and waterfall plot of the $\mathrm{d}I/\mathrm{d}V$ linecut along the red line in panel (a). The gap edge positions extracted from Dynes fitting of each spectrum are marked in panels (c) and (d), revealing high uniformity of the superconducting gap. For the data in panels (b)–(d), tunneling junction was stabilized with parameters of $V_{\mathrm{s}} = 1$ mV, $I_{\mathrm{t}} = 1$ nA, lock-in parameters were $V_{\mathrm{mod}} = 10$ μV and $f = 932$ Hz.

During the experiment, we find that the SC phase in β-$IrSn_4$ demonstrates exceptional sensitivity to magnetic fields, necessitating meticulous demagnetization of the instrumentation and sample to resolve the characteristic spectroscopic signatures. In magnetic-field-dependent experiments, the SC gap remains robust only for applied fields up to 6 mT. STS experiments across a large area further reveal the absence of vortices and the homogeneity of the SC. Notably, while ramping up and down the magnetic field or varying the scanning box, the SC gap exhibits a stochastic emergence and disappearance for fields below 6 mT, but remains remarkably consistent in both shape and magnitude whenever it is resolved (Fig. S4).

Assuming the system is a type-II SC, the theoretical density of quantum flux vortices n at an applied magnetic field of $B = 6$ mT is 2.90 $\mu\mathrm{m}^{-2}$. Given our typical large-scale scanning field of view (FOV) of 1.5 μm × 1.5 μm (yielding a total area of 2.25 $\mu\mathrm{m}^2$)), we would expect to observe approximately 6–7 vortices within a single FOV. Empirically, for a type-II SC approaching its upper critical field, the vortices become densely packed. Under such conditions, a significant portion of the scanning area would be occupied by vortex cores and their surrounding halos within the FOV, leading to heavily suppressed SC gaps or zero-bias peaks due to the vortex bound states during the STS measurements, which is inconsistent with our observation.

Instead, the behavior of the SC gaps under magnetic fields strongly suggests that the sample resides in the intermediate state of a type-I SC. Type-I SCs possess a positive surface en-

ergy between the normal and SC phases. Under a magnetic field below H_c, the system thermodynamically minimizes the interfacial area, driving a macroscopic or mesoscopic phase separation into coexisting normal puddles and SC domains in the presence of a finite demagnetization factor for bulk material. When the applied magnetic field is varied in proximity to H_c, the sample repeatedly transitions through this intermediate state. Notably, our STM scanning FOV is substantially smaller than the characteristic spatial extent of these macroscopic phase domains. Due to fluctuations of our magnetic field controller at the mT level, the spatial redistribution of the normal and SC regions after each field variation is intrinsically random, giving rise to the stochastic emergence and disappearance of the SC gap captured by the localized STS measurements. These results provide microscopic experimental evidence for the classification of β-$IrSn_4$ as a rare compound type-I superconductor with an ultralow critical field (~ 6.8 mT).[6–8]

We also confirmed that the SC gap remains unmodulated by structural and electronic heterogeneities such as the underlying atomic lattice, stripes of the layer-dependent uniaxial CDW, multiple types of defects, and terrace step edges (Figs. S5–S7). Characterized by a Ginzburg–Landau parameter $\kappa = \lambda/\xi < 1/\sqrt{2}$, type-I SCs have a substantially large coherence length ξ, which far exceeds the characteristic length scales of the CDW and other atomic-scale structural modulations ($\xi \gg \lambda_{CDW}$). Thus, the highly extended order parameter spatially averages out these localized charge density perturbations. This offers a plausible explanation for the observed homogeneity of the SC state.

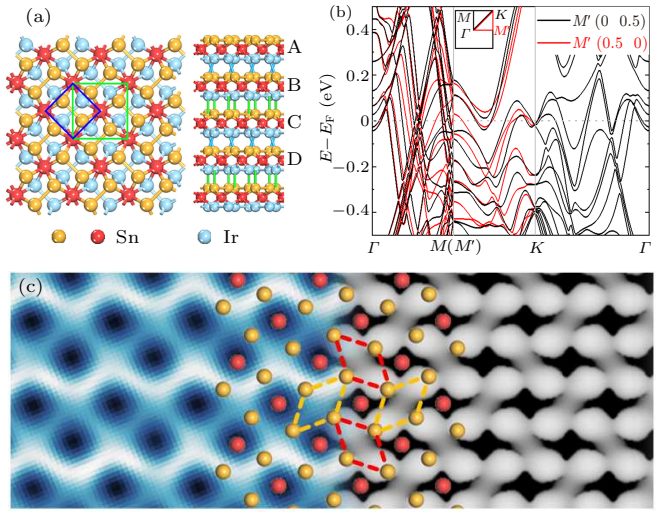


Fig. 4. Calculated configurations and electronic properties for the slab model. (a) Top and side views of the slab model. (b) Total band structures for the slab model with six $IrSn_4$ layers. (c) Atomically resolved experimental and simulated STM image at ~ 200 mV.

In order to understand the origin of the unconventional CDW pattern, we performed first-principles calculations by density functional theory (DFT). DFT calculations were performed in the Vienna *Ab initio* Simulation Package (VASP)[27,28] adopting the projector-augmented wave (PAW) method and the Perdew–Burke–Ernzerhof (PBE) [29] functional. The grimme-D3 method[30] was used to describe the van der Waals interaction between β-$IrSn_4$ layers.[31] A slab model containing six $IrSn_4$ layers was constructed to investigate the influence of interlayer interactions on surface electronic states. The vacuum layers for the slab models are larger than 15 Å. The atoms were fully relaxed until the force on each atom was less than 0.01 eV·Å^{-1} in all β-$IrSn_4$ systems. In Fig. 4(a), we provide the top and side views of this configuration. When only the top layer of the material is considered, the structure exhibits C_4 symmetry, meaning the material is identical along the a and b directions, which is also supported by the calculated band structure for the monolayer β-$IrSn_4$ (shown in Fig. S8). However, for the multilayer slab model, as shown in the side view of Fig. 4(a), the differences in interlayer interactions can be clearly observed. For instance, the orientation of adjacent Sn atoms between layers A and B (blue line) is at a 90° angle to that between layers B and C (green line). In this case, the entire system transforms to C_2 symmetry, which implies that the electronic structure may differ along the a and b directions. In Fig. 4(b), we provide the total band structures for the slab model containing six $IrSn_4$ layers. By comparing the bands along different directions (Γ–M vs Γ–M'), we can differentiate the bands shift due to the interlayer interactions from the second layer. In Fig. 4(c), we also present the simulated STM images, which clearly show good agreement with the experimental results and exhibit a transition from four-fold to two-fold symmetry, confirming that the emergence of CDW is induced by interlayer interactions.

In Fig. S9, we also performed density functional perturbation theory (DFPT) calculations to explore the potential BCS superconductivity of β-$IrSn_4$ via the QUANTUM ESPRESSO package.[32] The relativistic norm-conserving ONCV pseudopotentials [33] combined with the PBE exchange–correlation functional [29] were adopted. A plane-wave cutoff energy of 50 Ry, a k-mesh of $12 \times 12 \times 12$, and a Marzari–Vanderbilt smearing of 0.01 Ry were employed in calculating the electronic states. The dynamical matrices and EPC matrices were computed by density functional perturbation theory using a q-mesh of $3 \times 4 \times 2$. The Eliashberg spectral function $a^2F(\omega)$ was calculated by

$$a^2F(\omega) = \frac{1}{2\pi N(E_F)} \sum_{qv} \frac{\gamma_{qv}}{\omega_{qv}} \delta(\omega - \omega_{qv}), \tag{1}$$

where γ_{qv} is the phonon linewidth, ω_{qv} is the phonon eigen frequency, and $N(E_F)$ is the electronic DOS at the Fermi level. The projected phonon DOS and Eliashberg spectral function show that the transition metal Ir atoms make dominant contributions to the electron–phonon coupling (EPC) of β-$IrSn_4$.

The EPC constant λ was calculated by

$$\lambda = 2\int_0^{\infty} \frac{\alpha^2 F(\omega)}{\omega} \mathrm{d}\omega. \quad (2)$$

From this, we obtained a relatively strong EPC strength $\lambda = 0.365$. The superconducting critical temperature was estimated using the McMillan–Allen–Dynes formula[34]

$$T_c = \frac{\omega_{\log}}{1.2} \exp\left(-\frac{1.04(1+\lambda)}{\lambda - \mu^*(1+0.62\lambda)}\right), \quad (3)$$

where $\omega_{\log} = 249.65$ K is the logarithmic average of the phonon frequency, and μ^* is the effective Coulomb repulsion constant. Here, we obtained $\mu^* = 0.26N(0)/(1+N(0)) = 0.127$,[35] where $N(0) = 0.961$ eV^{-1} is the DOS per transition metal atom. We estimated a $T_c \sim 0.9$ K for bulk β-$IrSn_4$, which is close to the experimental result of 1.05 K.[7] This suggests that β-$IrSn_4$ is very likely to be a BCS superconductor. Due to the long distance between two nearest Ir layers (~ 5.9 Å), the influence of interlayer vibration on the superconductivity of β-$IrSn_4$ is relatively weak, which is confirmed by the experimental results, where the uniform SC gaps are found along the a and b directions.

In summary, we have performed an atomic-scale study of the noble-metal intermetallic superconductor β-$IrSn_4$ using ultra-low-temperature scanning tunneling microscopy and spectroscopy. We identify a uniaxial charge density wave that breaks the in-plane C_4 symmetry and, more importantly, exhibits a layer-by-layer alternation of orientation following the intrinsic stacking sequence, forming a layer-dependent uniaxial CDW. This alternating behavior is robust and closely tied to the crystallographic structure, indicating an intrinsic electronic order governed by interlayer coupling. Meanwhile, a homogeneous superconducting gap is observed to coexist with the CDW without detectable modulation, suggesting a weak coupling between the two orders. First-principles calculations reveal that interlayer interactions can induce the observed anisotropic electronic structure.

Acknowledgements

Project supported by the National Key Research and Development Program of China (Grant Nos. 2024YFA1207700, 2024YFA1207800, and 2022YFA1204100), the National Natural Science Foundation of China (Grant Nos. 62488201, 61925111, and U23A6015), the CAS Project for Young Scientists in Basic Research (Grant No. YSBR-003), the Youth Innovation Promotion Association (Grant No. 2023005), and the Quantum Science and Technology-National Science and Technology Major Project (Grant No. 2021ZD0302700).

References

[1] Shen D, Kuo C N, Yang T W, Chen I N, Lue C S and Wang L M 2020 *Commun. Mater.* **1** 56
[2] Zhu W, Song R, Huang J, *et al*. 2023 *Nat. Commun.* **14** 7012
[3] Ye Y, Song R, Xiao H, Xian G, Guo H, Yang H, Chen H and Gao H J 2024 *Nano Lett.* **24** 13455
[4] Xu C Q, Li B, Zhang L, Pollanen J, Yi X L, Xing X Z, Liu Y, Wang J H, Zhu Z, Shi Z X, Xu X and Ke X 2021 *Phys. Rev. B* **104** 125127
[5] García Talavera P, Moreno J A, Herrera E, Buzdin A I, Bud'ko S L, Canfield P C, Guillamón I and Suderow H 2025 *J. Supercond. Nov. Magn.* **38** 158
[6] Tran V H, Bukowski Z, Wiśniewski P, Tran L M and Zaleski A J 2013 *J. Phys.: Condens. Matter* **25** 155701
[7] Ahmad N, Shimada S, Hasegawa T, Suzuki H, Afzal M A, Nakamura N, Higashinaka R, Matsuda T D and Aoki Y 2024 *J. Phys. Soc. Jpn.* **93** 044706
[8] Speer S, Pershin Y V, Blawat J, Singleton J and Jin R 2026 *J. Phys.: Condens. Matter* **38** 055702
[9] Wu H, Hallas A M, Cai X, Huang J, Oh J S, Loganathan V, Weiland A, McCandless G T, Chan J Y, Mo S K, Lu D, Hashimoto M, Denlinger J, Birgeneau R J, Nevidomskyy A H, Li G, Morosan E and Yi M 2022 *npj Quantum Mater.* **7** 31
[10] Mai T L and Tran V H 2022 *RSC Adv.* **12** 17882
[11] Mun E, Ko H, Miller G J, Samolyuk G D, Bud'ko S L and Canfield P C 2012 *Phys. Rev. B* **85** 035135
[12] Wang Y J, Liang D D, Ge M, Yang J, Gong J X, Luo L, Pi L, Zhu W K, Zhang C J and Zhang Y H 2018 *J. Phys.: Condens. Matter* **30** 155701
[13] Li G, Fu C, Shi W, *et al*. 2019 *Angew. Chem., Int. Ed.* **58** 13107
[14] Satheasuweatha M N, Mariappan S, Maran T, Kuo C N, Lue C S, Sonachalam A and Joseph B 2025 *Phys. Status Solidi RRL* **19** 2500126
[15] Sahu S, Chen D, Heinsdorf N, Warner A N, Altthaler M, Singh A K, Bonn D A, Burke S A and Hallas A M 2025 *Commun. Mater.* **6** 244
[16] Nordmark E L, Wallner O and Häussermann U 2002 *J. Solid State Chem.* **168** 34
[17] Tranquada J M, Sternlieb B J, Axe J D, Nakamura Y and Uchida S 1995 *Nature* **375** 561
[18] Sipos B, Kusmartseva A F, Akrap A, Berger H, Forró L and Tutiš E 2008 *Nat. Mater.* **7** 960
[19] Chang J, Blackburn E, Holmes A T, Christensen N B, Larsen J, Mesot J, Liang R, Bonn D A, Hardy W N, Watenphul A, Zimmermann M V, Forgan E M and Hayden S M 2012 *Nat. Phys.* **8** 871
[20] Ghiringhelli G, Le Tacon M, Minola M, Blanco-Canosa S, Mazzoli C, Brookes N B, De Luca G M, Frano A, Hawthorn D G, He F, Loew T, Sala M M, Peets D C, Salluzzo M, Schierle E, Sutarto R, Sawatzky G A, Weschke E, Keimer B and Braicovich L 2012 *Science* **337** 821
[21] Comin R, Frano A, Yee M M, Yoshida Y, Eisaki H, Schierle E, Weschke E, Sutarto R, He F, Soumyanarayanan A, He Y, Le Tacon M, Elfimov I S, Hoffman J E, Sawatzky G A, Keimer B and Damascelli A 2014 *Science* **343** 390
[22] Chen H, Yang H, Hu B, *et al*. 2021 *Nature* **599** 222
[23] Teng X, Chen L, Ye F, *et al*. 2022 *Nature* **609** 490
[24] Yin J X, Jiang Y X, Teng X, *et al*. 2022 *Phys. Rev. Lett.* **129** 166401
[25] Shi X, Liu X, Li G, Zhao Z, Yang H, Lin X and Gao H J 2025 *Chin. Phys. B* **34** 077101
[26] Dynes R C, Narayanamurti V and Garno J P 1978 *Phys. Rev. Lett.* **41** 1509
[27] Kresse G and Hafner J 1993 *Phys. Rev. B* **47** 558
[28] Kresse G and Furthmüller J 1996 *Comput. Mater. Sci.* **6** 15
[29] Perdew J P, Burke K and Ernzerhof M 1996 *Phys. Rev. Lett.* **77** 3865
[30] Grimme S, Antony J, Ehrlich S and Krieg H 2010 *J. Chem. Phys.* **132** 154104
[31] Dion M, Rydberg H, Schröder E, Langreth D C and Lundqvist B I 2004 *Phys. Rev. Lett.* **92** 246401
[32] Giannozzi P, Baroni S, Bonini N, *et al*. 2009 *J. Phys.: Condens. Matter* **21** 395502
[33] Schlipf M and Gygi F 2015 *Comput. Phys. Commun.* **196** 36
[34] Allen P B and Dynes R C 1975 *Phys. Rev. B* **12** 905
[35] Zheng F, Li X B, Tan P, Lin Y, Xiong L, Chen X and Feng J 2020 *Phys. Rev. B* **101** 100505